



Anisotropic thermal expansion effects in layered *n*-Alkyl carboxylic acid – bipyridyl cocrystals

Amy V. Hall, Dmitry S. Yufit, Yingfeng Zhang, Osama M. Musa & Jonathan W. Steed

To cite this article: Amy V. Hall, Dmitry S. Yufit, Yingfeng Zhang, Osama M. Musa & Jonathan W. Steed (2021) Anisotropic thermal expansion effects in layered *n*-Alkyl carboxylic acid – bipyridyl cocrystals, *Supramolecular Chemistry*, 33:10, 578-585, DOI: [10.1080/10610278.2022.2117623](https://doi.org/10.1080/10610278.2022.2117623)

To link to this article: <https://doi.org/10.1080/10610278.2022.2117623>



© 2022 The Author(s). Published by Informa UK Limited, trading as Taylor & Francis Group.



[View supplementary material](#)



Published online: 05 Sep 2022.



[Submit your article to this journal](#)



Article views: 401



[View related articles](#)



[View Crossmark data](#)

Anisotropic thermal expansion effects in layered *n*-Alkyl carboxylic acid – bipyridyl cocrystals

Amy V. Hall ^a, Dmitry S. Yufit ^a, Yingfeng Zhang^a, Osama M. Musa ^b and Jonathan W. Steed ^a

^aDepartment of Chemistry, Durham University, Durham, UK; ^bAshland LLC, Bridgewater, New Jersey, USA

ABSTRACT

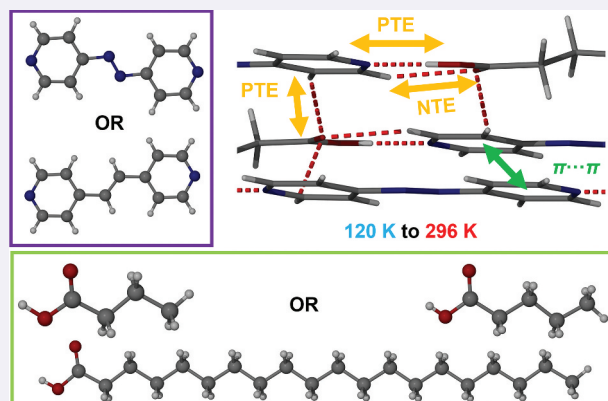
Cocrystallisation of butanoic acid (**BA**), pentanoic acid (**PA**), and eicosanoic acid (**EA**) with 4,4'-azopyridine (**azp**) and *trans*-1,2-bis(4-pyridyl)ethylene (**bpe**) results in 2:1 lamellar cocrystals. All cocrystals display the OH...N_{pyridyl} seven-membered ring supramolecular synthon however, each cocrystal responds differently upon heating. Positive thermal expansion (PTE) occurs along the *c*-axis due to π ... π stacking in the isostructural **BA** cocrystals, while the **PA** cocrystals are not isostructural and display a mixture of *anti* and *gauche* conformations of the acid chains because of the length mismatch with the coformer. **PA**₂-**azp** displays negative thermal expansion (NTE) of the intrasython C...O hydrogen bond. The two **EA** cocrystals both display *c*-axis elongation on warming due to the expansion of the distance between the alkyl chains. The expansion by more than 1 Å in **EA**₂-**azp** is highly anisotropic, however, there is much less *c*-axis expansion in **EA**₂-**bpe**.

ARTICLE HISTORY

Received 22 May 2022
Accepted 22 August 2022

KEYWORDS

thermal expansion; cocrystal; synthon; crystallisation



Introduction

The expansion of materials in response to an increase in temperature is typically caused by an increase in the magnitude and frequency of atomic vibrations [1, 2]. On a macroscopic scale, when unit cell axes increase upon heating, this is termed positive thermal expansion (PTE). Other types of thermal response include negative thermal expansion (NTE), and zero thermal expansion (ZTE), though they are less common [3–5]. PTE and NTE can be reversible or irreversible and can also occur in the same material [6]. Whether positive or negative thermal expansion is observed depends on the type of bonds within the material. For example, fewer and weaker intermolecular interactions in molecular solids give rise to positive thermal expansion [7], while thermal contraction typically occurs

due to hydrogen bond strengthening [8,9]. However, hydrogen bonding dimensionality alone is not a reliable predictor of thermal expansion behaviour [10]. In organic systems, both PTE and NTE have been reported in crystalline single component [11], and multicomponent systems, such as inclusion compounds [1,12,13], salts [2,14,15], hydrates [16,17], solvates [18], and cocrystals [6–8,19–28]. The anisotropic expansion of lamellar solids can give rise to considerable temperature-dependent changes in crystal packing environment, even in the absence of a first-order phase change [24]. Materials exhibiting NTE, ZTE, and PTE have applications in but are not limited to superconductors [29], ceramics [30], solar energy [31], and space science [6].

To investigate the thermal expansion in layered cocrystalline solids, we crystallised short- and long-

chain *n*-alkyl carboxylic acids with two different bipyridyl cofomers to explore the cocrystal response to increasing temperature in the solid state. The acids chosen represent a range of lengths to probe the relative effect of lamellar thickness as opposed to hydrogen bonded synthon. We used linear *n*-alkyl chains to promote lamellar packing since branched analogues are unlikely to pack efficiently side-by-side.

Results and discussion

Solution crystallisation of butanoic acid (**BA**), pentanoic acid (**PA**), and eicosanoic acid (**EA**) were undertaken with bifunctional pyridyl cofomers 4,4'-azopyridine (**azp**) and *trans*-1,2-bis(4-pyridyl)ethylene (**bpe**) (Figure 1). These compounds were chosen as they are likely to form layered solids[27], and as the acid substituents are different lengths, they should affect the layer size and the layered packing arrangement of the cocrystal. This kind of anisotropic structure may, in turn, result in differential thermal expansion effects. The shorter chain acid cocrystals are likely to be controlled by the cocrystal hydrogen OH...N_{pyridyl} supramolecular bonded synthon, while the longer chain acid cocrystal will be dominated by the packing behaviour of the long-chain alkyl substituents, in a similar way to previous work on a photoactive 25-carbon chain acid[28]. In each case, each monocarboxylic acid was combined with a pyridyl cofomer in a 2:1 molar ratio, respectively, which reflects the single hydrogen bond donor group of the acids and the two hydrogen bond acceptor groups of the pyridyl cofomer. The mixtures were briefly sonicated and allowed to stand to bring about slow evaporation of the solvent under ambient conditions. These experiments resulted in six cocrystals characterised by single-crystal X-ray diffraction (SC-XRD)

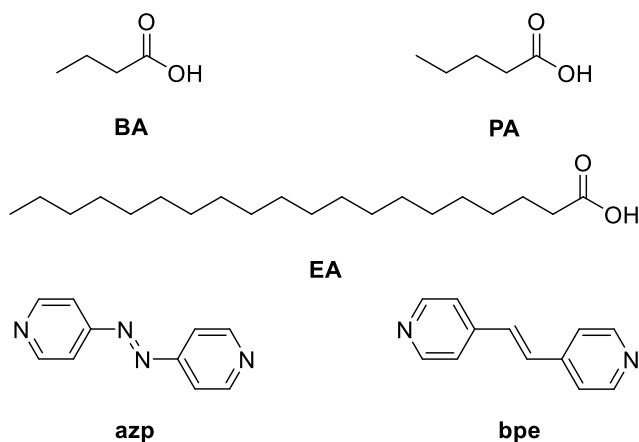


Figure 1. The compound key for the *n*-alkyl carboxylic acids and bifunctional pyridyl cofomers.

consisting of **BA**₂·**azp**, **BA**₂·**bpe**, **PA**₂·**azp**, **PA**₂·**bpe**, **EA**₂·**azp**, and **EA**₂·**bpe**.

All cocrystals crystallise in the centrosymmetric, triclinic *P* $\bar{1}$ space group and display OH...N hydrogen bonds from the carboxylic acid hydrogen atom of the acid to the pyridyl nitrogen atom of the cofomer. A weaker CH...O interaction also occurs from the C-H of the pyridyl ring to the carbonyl oxygen atom of the acid, to complete the hydrogen-bonded dimer R₂²(7) motif[32]. Two additional weak CH...O hydrogen bonds also occur between layers from the C-H groups of the pyridyl rings to the carbonyl oxygen atom on an adjacent acid molecule, which adds dimensionality to the cocrystal layers. The cocrystal hydrogen-bonded layers rest diagonally between the *b* and *c* axes, with the intermolecular hydrogen bonds within the acid-pyridyl synthon occurring along the *b*-axis. The cocrystals were characterised at 120 K and then warmed to near room temperature to investigate their thermal response. All hydrogen bond distances reported are measured from the hydrogen bond donor atom to the hydrogen bond acceptor (O...N or C...O) and not from or to the H atom, as the position of the H atoms cannot be located with high precision in high-temperature structures.

Single crystal x-ray diffraction

BA₂·**azp** and **BA**₂·**bpe**

The cocrystals **BA**₂·**azp** and **BA**₂·**bpe** are isostructural (Figure 2). Both materials show negligible changes in the *a* and *b*-axes, but significant PTE in the *c*-axis upon warming (elongation of 0.76 Å and 0.87 Å, respectively), caused by expansion in the face-to-face π...π stacking interactions aligned along the *c*-axis which expand on warming by 0.14 and 0.093 Å for both cocrystals, respectively (Table 1). The given π...π stacking interaction distances are the distances between centroids of adjacent pyridyl rings. The positive correlation between π...π stacking direction and thermal expansion direction has been observed in similar cocrystal systems [27,33]. The strong OH...N hydrogen bonds in the hydrogen-bonded sheet show insignificant PTE upon warming (0.011 and 0.0057 Å for **BA**₂·**azp** and **BA**₂·**bpe**, respectively). Strong intermolecular interactions are rarely significantly perturbed on warming, unlike weaker intra- and intersynthon CH...O hydrogen bonds [9,20,24,33]. This is demonstrated by the 0.098 (within the acid-pyridyl synthon), 0.094 and 0.039 (intersynthon) Å PTE in CH...O hydrogen bonds in **BA**₂·**azp** and the 0.13 (intrasynthon), 0.099 and 0.042 (intersynthon) Å PTE in **BA**₂·**bpe**. Therefore, in this instance, the bispyridyl cofomer does not affect the thermal expansion properties of either cocrystal of **BA**.

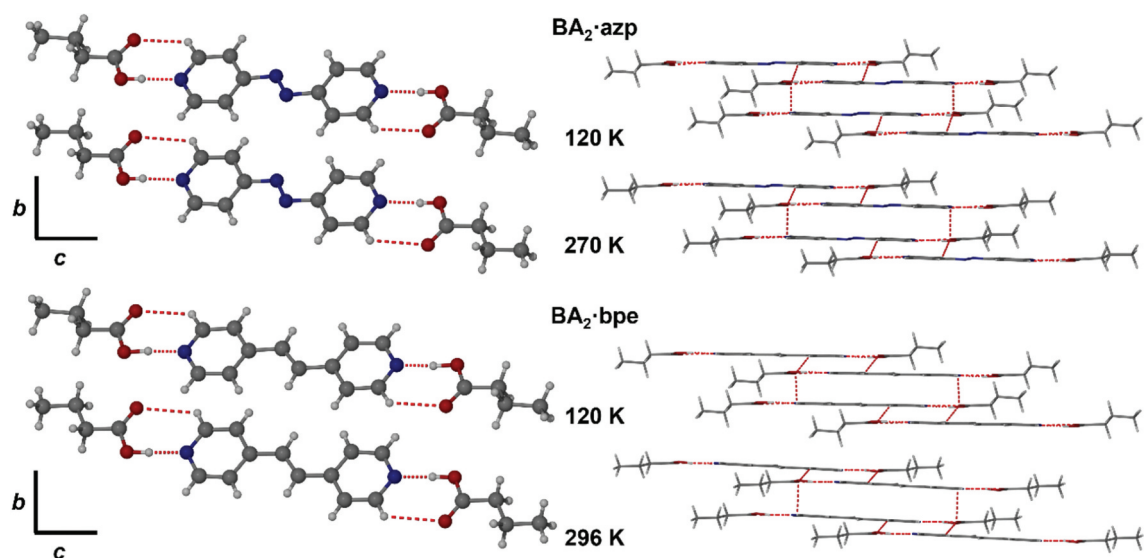


Figure 2. The X-ray structures and packing diagrams of **BA₂·azp** and **BA₂·bpe** at 120, 270 (**BA₂·azp**) and 296 (**BA₂·bpe**) K.

Table 1. The unit cell parameters, hydrogen bond distances, and π – π stacking distances of **BA₂·azp** and **BA₂·bpe** at 120, 270 (**BA₂·azp**) and 296 (**BA₂·bpe**) K.

Cocrystal Temperature /K	BA ₂ ·azp			BA ₂ ·bpe		
	120	270	% Change	120	296	% Change
<i>a</i> -axis /Å	6.6795(2)	6.6930(3)	0.20	6.5688(4)	6.5059(4)	−0.96
<i>b</i> -axis /Å	6.9217(2)	6.9135(4)	−0.12	6.9189(4)	6.9893(5)	1.02
<i>c</i> -axis /Å	11.3594(4)	12.1182(6)	6.68	11.4828(7)	12.3559(8)	7.60
Unit cell volume /Å ³	469.70(3)	493.66(4)	5.10	475.61(5)	503.90(6)	5.95
O...N /Å	2.6804(14)	2.691(3)	0.40	2.6583(13)	2.664(3)	0.21
C...O intralayer /Å	3.2191(19)	3.317(4)	3.04	3.2540(16)	3.384(4)	4.00
C...O interlayer /Å	3.1407(14) and 3.3523(18)	3.235(3) and 3.391(4)	3.00 and 1.15	3.1720(12) and 3.3572(14)	3.271(3) and 3.399(3)	3.12 and 1.25
π – π distance /Å	3.511	3.604	2.65	3.533	3.672	3.93

PA₂·azp and PA₂·bpe

Unlike the cocrystals of **BA**, **PA₂·azp** and **PA₂·bpe** are not isostructural (Figure 3). **PA₂·azp** is a conformational isomorph with two conformationally different molecules of **PA** in the asymmetric unit. One of the **PA** molecules is in an *anti*-conformation and the other is *gauche*. A twist in the N=N group, causes the **azp** molecule to be non-planar. The presence of two independent **PA** molecules results in two different values for the OH...N, CH...O intra- and intersynthon hydrogen

bond distances. In contrast, **PA₂·bpe** has only one unique molecule of **PA** in its asymmetric unit ($Z' = 0.5$) and exists in a *gauche* conformation, with a planar **bpe** cofomer situated on an inversion centre. The **BA** and **PA** cocrystals only differ by a single carbon atom however this aspect markedly affects the structures and unit cell parameters (Table 2) and seems to arise from a mismatch in the length of **PA** and the co-formers, whereas two **BA** molecules are good size match for the cofomers.

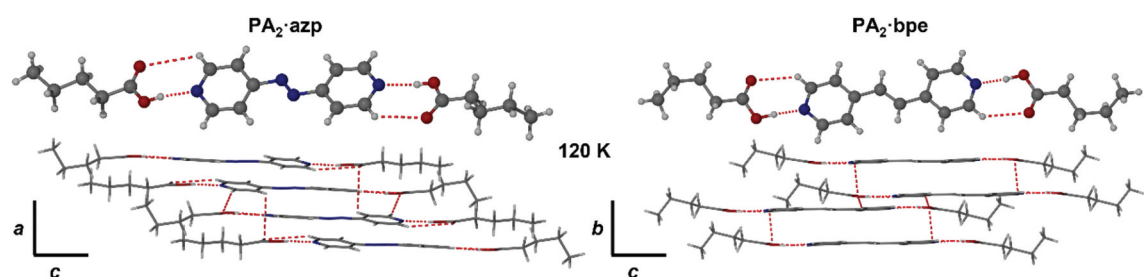


Figure 3. The X-ray structures and packing diagrams of **PA₂·azp** and **PA₂·bpe** at 120 K.

Table 2. The unit cell parameters, hydrogen bond distances, and π – π stacking distances of **PA₂·azp** and **PA₂·bpe** at 120 K and 293 (**PA₂·azp**) and 296 (**PA₂·bpe**) K.

Cocrystal Temperature /K	PA ₂ ·azp			PA ₂ ·bpe		
	120 K	293 K	% Change	120 K	296 K	% Change
a-axis /Å	7.1308(5)	7.326(2)	2.74	6.8211(5)	6.7511(18)	–1.03
b-axis /Å	10.4524(8)	10.505(3)	0.50	7.1875(6)	7.253(2)	0.91
c-axis /Å	14.8159(9)	15.161(5)	2.33	11.8334(10)	12.826(4)	8.39
Unit cell volume /Å ³	1035.87(13)	1115.6(6)	7.70	515.24(7)	558.8(3)	8.45
O...N /Å	2.644(4) and 2.729(4)	2.662(12) and 2.721(13)	0.68 and 0.29	2.6725(15)	2.687(4)	0.54
C...O intralayer /Å	3.303(4) and 3.597(4)	3.296(14) and 3.477(13)	0.21 and –3.34	3.2772(18)	3.372(5)	2.89
C...O interlayer /Å	3.272(4) and 3.277(4)	3.281(15) and 3.342(13)	0.28 and 1.98	3.3329(13) and 3.4238(15)	3.385(4) and 3.399(4)	1.56 and 0.72
π – π distance /Å	3.596	3.796	5.56	3.532	3.659	3.60

When the cocrystals were warmed to room temperature, the crystal quality of **PA₂·azp** and **PA₂·bpe** deteriorated significantly and the resulting structure determinations are of low precision with disorder of the terminal methyl groups. However, the unit cell parameters are unambiguous and give insight into the changes in the structure on warming. For **PA₂·azp** the *a*-axis increases by 0.20 Å, whereas the *a*-axis in **PA₂·bpe** decreases slightly in length upon warming, with a NTE of –0.07 Å. The *b*-axis in **PA₂·azp** and **PA₂·bpe** shows almost no PTE with the axis lengths increasing on warming by 0.053 and 0.070 Å, respectively. However, **PA₂·azp** shows a much smaller PTE in the *c*-axis when compared to **PA₂·bpe** (with increases of 0.35 and 1.00 Å, respectively), despite the π – π stacking interaction distance increasing by a similar amount in **PA₂·azp** (0.20 Å) and **PA₂·bpe** (0.19 Å). There is a significant offset of the pyridyl rings centroids in **PA₂·azp**, with a shift distance of 0.74 Å, compared to the offset of the rings in **PA₂·bpe** with an offset of only 0.019 Å. The offset of the pyridyl ring centroids is linked to the NTE observed in the intrasython CH...O hydrogen bond distances in **PA₂·azp**, which contract slightly on warming. For the stronger OH...N hydrogen bond along the same axis, the interactions increase by 0.018 and 0.008 Å on warming. The weak intersynthon CH...O hydrogen bonds of **PA₂·azp** increase by 0.009 and 0.065 Å. Cocrystal **PA₂·bpe** behaves differently to **PA₂·azp** in response to increasing temperature. **PA₂·bpe** has a much smaller PTE with an increase of 0.015 Å for the OH...N hydrogen bonds, 0.095 Å for intrasython CH...O hydrogen bonds, and PTE and NTE for the intersynthon CH...O hydrogen bonds at 0.052 and –0.025 Å.

In summary, the differences in the thermal expansion properties between **PA₂·azp** and **PA₂·bpe** on warming are due to the NTE observed in the intrasython CH...O

hydrogen bond interactions in **PA₂·azp**, causing the centroid distances of the pyridyl rings to have a greater offset. **PA₂·bpe** does not display the same thermal expansion properties.

EA₂·azp and EA₂·bpe

The two long-chain **EA** cocrystals, **EA₂·azp** and **EA₂·bpe** are not isostructural, even though the alkyl chains of the acid for both cocrystals are in an *anti*-conformation at both 120 K and room temperature (Figure 4). We note in passing that this is the first single-crystal diffraction study of this surfactant-like acid. On warming to room temperature, the *c*-axis lengths in **EA₂·azp** and **EA₂·bpe** expand by 1.04 and 0.13 Å, respectively. This represents a marked difference in two similar materials even given the temperature differences. In contrast, the *a*-axis length increase for **EA₂·azp** on warming is only 0.035 Å compared to 0.11 Å and for **EA₂·bpe** (Table 3). The *b*-axes only increase by 0.057 and 0.074 Å on warming for **EA₂·azp** and **EA₂·bpe**, respectively. The strong OH...N hydrogen bonds show negligible thermal expansion at 0.011 Å for **EA₂·azp** and 0.003 Å for **EA₂·bpe**. The intra- and intersynthon CH...O hydrogen bonds also show small PTE upon warming, with **EA₂·azp** showing CH...O bond distance changes of 0.048 (intrasython) and 0.038 and 0.094 Å (intersynthon), while **EA₂·bpe** has intrasython CH...O bond distance increases of 0.028 Å and intersynthon CH...O distances of 0.081 and 0.093 Å upon warming. No π – π stacking interactions are present in either **EA** cocrystal, as the distances between pyridyl rings of adjacent layers are too great to form a significant interaction, therefore, π -stacking interactions cannot account for the PTE observed in the *c*-axis of **EA₂·azp**.

The differences in thermal expansion properties in the two **EA** cocrystals must be due to differences in the cofomer, even though they are of a similar size and shape. **Azp** and **bpe** are known to undergo molecular pedal motion at different temperatures, resulting in disorder that is either dynamic or static [24,26,34–37].

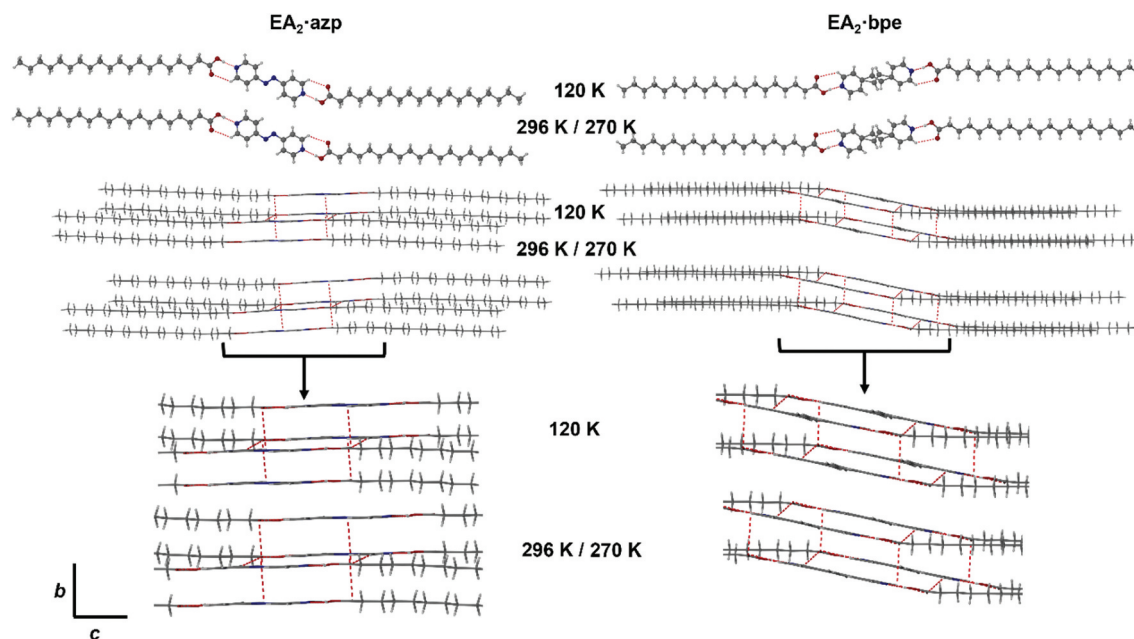


Figure 4. The X-ray structures and packing diagrams of **EA₂·azp** and **EA₂·bpe** at 120, 270 (**EA₂·bpe**), and 296 (**EA₂·azp**) K. A cross-section of the hydrogen-bonded network is enlarged for both crystals.

Table 3. The unit cell parameters, hydrogen bond distances, and $\pi\cdots\pi$ stacking distances of **EA₂·azp** and **EA₂·bpe** at 120, 270 (**EA₂·bpe**), and 296 (**EA₂·azp**) K.

Cocrystal Temperature /K	EA ₂ ·azp			EA ₂ ·bpe		
	120 K	296 K	% Change	120 K	270 K	% Change
a-axis /Å	5.460(3)	5.4949(6)	0.64	4.8640(3)	4.9744(6)	2.27
b-axis /Å	6.853(3)	6.9098(6)	0.83	6.8573(4)	6.9314(8)	1.08
c-axis /Å	33.412(18)	34.451(4)	3.11	36.699(2)	36.833(4)	0.37
Unit cell volume /Å ³	1199.5(11)	1259.2(2)	4.98	1203.27(13)	1252.5(3)	4.09
O···N /Å	2.679(4)	2.690(8)	0.41	2.636(3)	2.639(4)	0.11
C···O intralayer /Å	3.289(5)	3.337(10)	1.46	3.484(3)	3.512(4)	0.80
C···O interlayer /Å	3.191(5) and 3.623(5)	3.229(11) and 3.717(10)	1.19 and 2.60	3.234(2) and 3.410(3)	3.315(4) and 3.503(4)	2.51 and 2.73

Interestingly, the **EA₂·bpe** structure displays disorder of the central ethylene group of **bpe**. As the site occupancies of the disordered atoms remain constant with temperature, the disorder is likely to be static [26,38]. In contrast, the **EA₂·azp** is ordered. The long *c* axis in both structures encompasses the side-by-side packing of the long alkyl chains with the **EA** molecular axis orientated at about 50° to this axis in each case. Interestingly, while the ordered **EA₂·azp** structure has almost coplanar seven-membered ring synthons and alkyl substituents, the disordered **EA₂·bpe** structure has a wave-like arrangement in which there is an offset of the alkyl substituents. As temperature increases, the distance between adjacent alkyl chains expands. This expansion seems to be tolerated in the wavelike **bpe** structure resulting in more isotropic expansion, while in the **azp** structure all the expansion is focused along the *c* axis. Increased thermal motion in

hydrogen-bonded solids has been shown to result in significant thermally induced motion previously [28,39].

Powder x-ray diffraction

The X-ray powder diffraction (XRPD) patterns calculated from the low-temperature SC-XRD data of the cocrystal structures reveal significant differences when compared to the experimental room temperature patterns of the same cocrystals (Figures 5 and S1-5). In all cases, the calculated room temperature patterns have an improved fit to the experimental data in comparison to the patterns derived from the low-temperature data and confirm that the single crystals are representative of the bulk, although some differences remain which appear to arise from very significant preferred orientation (Table S1), particularly in

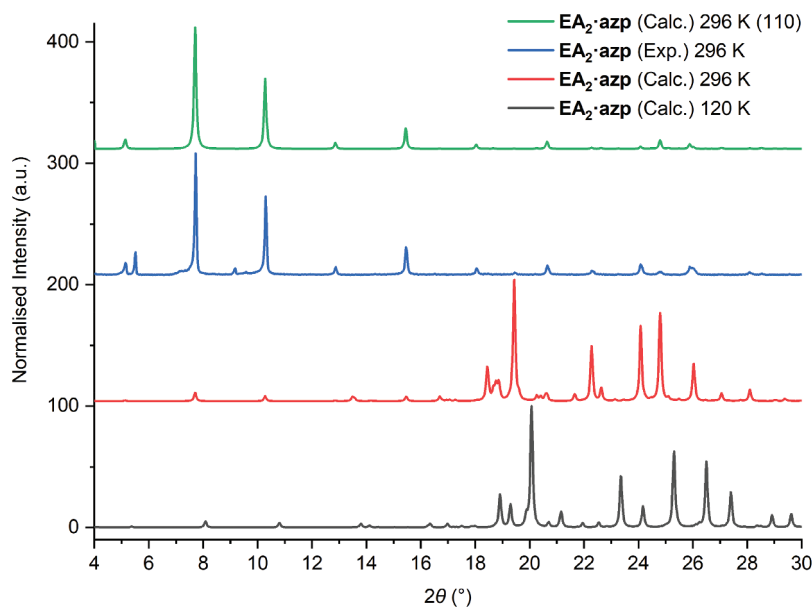


Figure 5. The low and room temperature calculated and experimental PXRD patterns of **EA₂·azp** highlighted severe (110) preferred orientation. The experimental pattern displays trace impurity peaks at 5.5 and 9.2 2θ .

the case of **EA₂·azp** which showed severe (110) preferred orientation (Figure 5).

Conclusion

Six binary pyridyl-acid cocrystals involving the OH...N_{pyridyl} seven-membered ring supramolecular synthon have been prepared. All cocrystals crystallise in the triclinic $P\bar{1}$ space group and form a 2D hydrogen-bonded network via CH...O interactions. Upon warming, all cocrystals show anisotropic thermal expansion effects to different degrees. The **BA** cocrystals expand in the *c*-axis due to π ... π stacking interactions that run along the same axis, while the **PA** cocrystals display PTE, partly due to differences in the *gauche* conformations of the **PA** chains. However, **PA₂·azp** displays NTE in the intrasynthon CH...O hydrogen bonds on warming, which causes the pyridyl centroid distances to be further offset. Both **EA** cocrystals show *c*-axis expansion due to increased motion of the alkyl substituents that is focused almost entirely along *c* for the ordered **azp** cocrystal but the disordered **EA₂·bpe** shows more isotropic expansion. Therefore, in anisotropic layered solids, thermal effects can give rise to considerable differences in the expansion of each crystallographic axis. These effects, in turn, can give rise to very different experimental XRPD patterns compared to those calculated from low-temperature single-crystal data, particularly when significant preferred orientation effects are also present.

Experimental

All reagents and solvents were purchased from standard commercial sources and used without further purification. X-ray powder diffraction patterns were recorded on glass slides using a Bruker AXS D8 Advance diffractometer with a Lynxeye Soller PSD detector, using Cu K α radiation at a wavelength of 1.5406 Å. CHN analysis was undertaken using an Exeter CE-440 Elemental Analyser. CN analysis was undertaken using a Costech ECS 4010 Elemental Analyser. Single crystal data were collected on Bruker D8 Venture 3-circle diffractometers at various configurations (Photon 100 CMOS detector, 1 μ S-microsource focusing mirrors/Photon III MM C14 CPAD detector, 1 μ S-III-microsource, focusing mirrors) equipped with Cryostream (Oxford Cryostreams) open-flow nitrogen cryostats and using MoK α radiation with a wavelength of 0.71073 Å (CuK α radiation, $\lambda = 1.54178$ Å for the **EA₂·azp** high-temperature structure). All structures were solved using direct methods and refined by full-matrix least squares on F^2 for all data using SHELXL [40] and OLEX2 [41] software. All non-hydrogen atoms were refined with anisotropic displacement parameters. CH hydrogen atoms were placed in calculated positions and refined in riding mode. H atoms attached to oxygen atoms were located on the difference map when possible or placed in calculated positions.

Note that high-temperature data for **BA₂·azp** was recorded at 270 K because of the instability of the crystal at room temperature, similarly, the **EA₂·bpe** structure could not be determined higher than

270 K due to decreasing crystal quality on warming. Experimental procedure and crystal details for individual cocrystals at 120 K and room temperature can be found in the Supporting Information. CCDC deposition numbers: 2,171,654–2,171,666. Crystals of an impurity mono-chloro azopyridine [1] were also characterised and the structure is discussed in the supplementary information. Crystals of an impurity mono-chloro azopyridine (chlorinated azopyridined have been observed previously as impurities in azopyridine [42]) were also characterised and the structure is discussed in the supplementary information.

Acknowledgments

We thank Ashland LLC and the Engineering and Physical Sciences Research Council for studentship funding. We also thank Dr Darren R. Gröcke for the CN analysis of samples at the Stable Isotope Biogeochemistry Laboratory at Durham University.

Disclosure statement

No potential conflict of interest was reported by the author(s).

Funding

This work was funded by Ashland LLC and the Engineering and Physical Sciences Research Council.

ORCID

Amy V. Hall  <http://orcid.org/0000-0002-3664-9229>
 Dmitry S. Yufit  <http://orcid.org/0000-0002-7208-1212>
 Osama M. Musa  <http://orcid.org/0000-0002-1110-1582>
 Jonathan W. Steed  <http://orcid.org/0000-0002-7466-7794>

Data Availability Statement

Electronic supplementary information (ESI) available: XRPD, preferred orientation details, and experimental details. CCDC 2171654-2171666. Other data is available from the authors.

References

- [1] Engel ER, Smith VJ, Bezuidenhout CX, et al. Thermoresponsive organic inclusion compounds: modification of thermal expansion behavior by simple guest replacement. *Chem. Mater.* **2016**;28(14):5073–5079.
- [2] Dwivedi B, Shrivastava A, Negi L, et al. Colossal positive and negative axial thermal expansion induced by scissor-like motion of a two-dimensional hydrogen bonded network in an organic salt. *Cryst. Growth Des.* **2019**;19(5):2519–2524.
- [3] Goodwin AL. The ins and outs of thermal expansion. *Nat. Nanotechnol.* **2008**;3(12):711–712.
- [4] Lind C. Two decades of negative thermal expansion research: where do we stand? *Materials.* **2012**;5(12):1125–1154.
- [5] Goodwin AL. Packing down. *Nat. Mater.* **2010**;9(1):7–8.
- [6] Das D, Jacobs T, Barbour LJ. Exceptionally large positive and negative anisotropic thermal expansion of an organic crystalline material. *Nat. Mater.* **2010**;9(1):36–39.
- [7] Vu TH, Maynard-Casely HE, Cable ML, et al. Anisotropic thermal expansion of the acetylene–ammonia co-crystal under Titan’s conditions. *J. Appl. Crystallogr.* **2020**;53(6):1524–1530.
- [8] Ding XD, Unruh DK, Groeneman RH, et al. Controlling thermal expansion within mixed cocrystals by tuning molecular motion capability. *Chem. Sci.* **2020**;11(29):7701–7707.
- [9] Saha BK. Thermal expansion in organic crystals. *J. Indian Inst. Sci.* **2017**;97(2):177–191.
- [10] Bhattacharya S, Saraswatula VG, Saha BK. Does higher-dimensional hydrogen bonding guarantee a smaller thermal expansion? A thermal expansion study of an interdigitated 1D and interpenetrated 3D hydrogen-bonded colored dimorphic system. *Cryst. Growth Des.* **2016**;16(1):277–284.
- [11] Dutta S, Munshi P. Unusual anisotropic thermal expansions with reversible axial switching and record-wide thermal hysteresis in single-component purely organic molecular crystals. *J Phys Chem C.* **2020**;124(50):27413–27421.
- [12] Engel ER, Smith VJ, Bezuidenhout CX, et al. Uniaxial negative thermal expansion facilitated by weak host–guest interactions. *Chem Commun.* **2014**;50(32):4238–4241.
- [13] Zakrzewski M, White MA, Abriel W. Influence of guest molecular species on the thermal expansion of clathrates of Dianin’s compound and concomitant anharmonic interactions. *J. Phys. Chem.* **1990**;94(5):2203–2206.
- [14] de Pedro I, Garcia-Saiz A, Dupont J, et al. On the colossal and highly anisotropic thermal expansion exhibited by imidazolium salts. *Cryst. Growth Des.* **2015**;15(11):5207–5212.
- [15] Szafranski M. Strong negative thermal expansion and relaxor ferroelectricity driven by supramolecular patterns. *J Mater Chem C.* **2013**;1(47):7904–7913.
- [16] Fortes AD, Suard E, Knight KS. Negative linear compressibility and massive anisotropic thermal expansion in methanol monohydrate. *Science.* **2011**;331(6018):742–746.
- [17] Birkedal H, Schwarzenbach D, Pattison P. Observation of Uniaxial Negative Thermal Expansion in an Organic Crystal We thank the staff of the Swiss–Norwegian Beam Line for their kind assistance and the Swiss National Science Foundation for financial support. H. B. thanks the Danish Research Agency for further financial support. *Angew. Chem, Int. Ed.* **2002**;41(5):754–756.
- [18] Montejo-Bernardo J, Garcia-Granda S. Negative thermal expansion in several solvated crystals form of an organic compound. *Acta Crystallogr, Sect. A: Found. Adv.* **2007**;63(a1):S206–S206.
- [19] Bhattacharya S. Interaction dependent anisotropic thermal expansion of a hydrogen bonded cocrystal. *J. Mol. Struct.* **2020**;1220:1–6.
- [20] Hutchins KM, Groeneman RH, Reinheimer EW, et al. Achieving dynamic behaviour and thermal expansion in the organic solid state via co-crystallization. *Chem. Sci.* **2015**;6(8):4717–4722.

- [21] Hutchins KM, Kummer KA, Groeneman RH, et al. Thermal expansion properties of three isostructural co-crystals composed of isosteric components: interplay between halogen and hydrogen bonds. *CrystEngComm*. **2016**;18(43):8354–8357.
- [22] Alimi LO, Lama P, Smith VJ, et al. Large volumetric thermal expansion of a novel organic cocrystal over a wide temperature range. *CrystEngComm*. **2018**;20(5):631–635.
- [23] Jones RH, Knight KS, Marshall WG, et al. Colossal thermal expansion and negative thermal expansion in simple halogen bonded complexes. *CrystEngComm*. **2014**;16(2):237–243.
- [24] Hutchins KM, Unruh DK, Verdu FA, et al. Molecular pedal motion influences thermal expansion properties within isostructural hydrogen-bonded co-crystals. *Cryst Growth Des*. **2018**;18(2):566–570.
- [25] Hutchins KM, Unruh DK, Carpenter DD, et al. Thermal expansion along one-dimensional chains and two-dimensional sheets within co-crystals based on halogen or hydrogen bonds. *CrystEngComm*. **2018**;20(45):7232–7235.
- [26] Juneja N, Unruh DK, Bosch E, et al. Effects of dynamic pedal motion and static disorder on thermal expansion within halogen-bonded co-crystals. *New J. Chem*. **2019**;43(47):18433–18436.
- [27] Ding XD, Juneja N, Crawford AW, et al. Influence of multiple hydrogen bonds on thermal expansion within and between two-dimensional hydrogen-bonded sheets. *Cryst. Growth Des*. **2019**;19(12):7380–7384.
- [28] Hall AV, Yufit DS, Apperley DC, et al. The crystal engineering of radiation-sensitive diacetylene cocrystals and salts. *Chem. Sci*. **2020**;11(30):8025–8035.
- [29] Chen J, Hu L, Deng JX, et al. Negative thermal expansion in functional materials: controllable thermal expansion by chemical modifications. *Chem. Soc. Rev*. **2015**;44(11):3522–3567.
- [30] Shi NK, Song YZ, Xing XR Negative thermal expansion in framework structure materials, et al. *Coord. Chem. Rev*. **2021**;449:214204.
- [31] Yamamoto N, Gdoutos E, Toda R, et al. Thin films with ultra-low thermal expansion. *Adv. Mater*. **2014**;26(19):3076–3080.
- [32] Bernstein J, Davis RE, Shimoni L, et al. Patterns in hydrogen bonding: functionality and graph set analysis in crystals. *Angew. Chem, Int. Ed*. **1995**;34(15):1555–1573.
- [33] Ding XD, Crawford AW, Derrick WP, et al. Thermal expansion properties and mechanochemical synthesis of stoichiometric cocrystals containing tetrabromobenzene as a hydrogen- and halogen-bond donor. *Chem. - Eur. J*. **2021**;27(66):16329–16333.
- [34] Harada J, Ogawa K. Invisible but common motion in organic crystals: a pedal motion in stilbenes and azobenzenes. *J. Am. Chem. Soc*. **2001**;123(44):10884–10888.
- [35] Juneja N, Zahid E, Unruh DK, et al. Solid-state behaviors of imines: colossal biaxial positive thermal expansion, motion capability, and phase transitions. *CrystEngComm*. **2021**;23(25):4439–4443.
- [36] Crawford AW, Groeneman RH, Unruh DK Cooling-rate dependent single-crystal-to-single-crystal phase transition in an organic co-crystal, et al. *Chem Commun*. **2019**;55:3258–3261.
- [37] Harada J, Ogawa K. What molecules are likely or unlikely to undergo pedal motions in crystals? *Cryst. Growth Des*. **2014**;14(10):5182–5188.
- [38] Harada J, Ogawa K. Pedal motion in crystals. *Chem. Soc. Rev*. **2009**;38(8):2244–2252.
- [39] Calleja M, Mason SA, Prince PD Anisotropic thermal expansion in 18-crown-6. 2 H₂O. 2 HNO₃, et al. *New J. Chem*. **2003**;27:28–31.
- [40] Sheldrick GM. Crystal structure refinement with SHELXL. *Acta Crystallogr., Sect. C: Struct. Chem*. **2015**;71(1):3–8.
- [41] Dolomanov OV, Bourhis LJ, Gildea RJ, et al. OLEX2: a complete structure solution, refinement and analysis program. *J. Appl. Crystallogr*. **2009**;42(2):339–341.
- [42] Mazzeo PP, Carraro C, Arns A, et al. Diversity through similarity: a world of polymorphs, solid solutions, and cocrystals in a vial of 4,4'-diazopyridine. *Cryst. Growth Des*. **2020**;20(2):636–644.